Interaction and rheology of vesicle suspensions in confined shear flow

Zaiyi Shen, Alexander Farutin, Marine Thiébaud, and Chaouqi Misbah
Université Grenoble Alpes, LIPHY, F-38000, Grenoble, France
and CNRS, LIPHY, F-38000, Grenoble, France
(Received 20 June 2016; published 6 October 2017)

Dynamics and rheology of a confined suspension of vesicles (a model for red blood cells) are studied numerically in two dimensions by using an immersed boundary lattice Boltzmann method. We pay particular attention to the link between the spatiotemporal organization and the rheology of the suspension. Besides confinement, we analyze the effect of concentration of the suspension, ϕ (defined as the area fraction occupied by the vesicles in the simulation domain), as well as the viscosity contrast λ (defined as the ratio between the viscosity of the fluid inside the vesicles, η_{int}, and that of the suspending fluid, η_{ext}). The hydrodynamic interaction between two vesicles is shown to play a key role in determining the spatial organization. For $\lambda = 1$, the pair of vesicles settles into an equilibrium state with constant interdistance, which is regulated by the confinement. The equilibrium interdistance increases with the gap between walls, following a linear relationship. However, no stable equilibrium interdistance between two tumbling vesicles is observed for $\lambda = 10$. A quite ordered suspension is observed concomitant with the existence of an equilibrium interdistance between a vesicle pair. However, a disordered suspension prevails when no pair equilibrium interdistance exists, as occurs for tumbling vesicles. We then analyze the rheology, focusing on the effective viscosity, denoted as η, as well as on normalized viscosity, defined as $[\eta] = (\eta - \eta_{\text{ext}})/(\eta_{\text{ext}}\phi)$. Ordering of the suspension is accompanied by a nonmonotonic behavior of $[\eta]$ with ϕ, while η exhibits plateaus. The nonmonotonic behavior of $[\eta]$ is suppressed when a disordered pattern prevails.

DOI: 10.1103/PhysRevFluids.2.103101

I. INTRODUCTION

Blood is a dense suspension of red blood cells (RBCs), which account for around 45% of its total volume. Blood microstructure (RBC shapes and spatiotemporal distribution) strongly depends on flow conditions, such as local shear rate, flow curvature, and vessel-cell size ratio [1–5]. Rheological properties of blood are basically governed by RBC dynamics and their mutual interactions, which are closely related to the mechanical properties of RBCs. These are not yet fully quantified, in part due to the complexity of the internal structure of the RBCs. RBCs are made of a membrane enclosing a hemoglobin solution. The membrane is mainly a phospholipid bilayer having a cytoskeleton (a network of proteins, mostly spectrin) beneath. The bilayer has a very high resistance to dilatation, rendering the membrane virtually inextensible under practical loads. The cytoskeleton endows RBCs with resistance to bending and shearing deformations. Two biomimetic systems are widely used as a simplified model for RBC membrane: vesicles and capsules. The former are made of a phospholipid bilayer, devoid of cytoskeleton, and thus are inextensible and resist bending deformations but have no resistance to shear. The latter have an elastic membrane made of polymer networks with finite resistance to bending, shearing, and dilatation. Despite the disparities in structure and composition, these two systems share several common features with RBCs, such as tank treading and tumbling under shear flow or slipper and parachute shapes under pressure-driven flow, as discussed in a review [5].

The dynamics of a single deformable particle (RBC, vesicle, capsule) is relatively well understood thanks to a series of theoretical [6–12], experimental [13–16], and numerical [17–27] studies (see also reviews [5,28–30]). For example, the typical motions of RBCs in simple shear flow, namely, tank treading, tumbling, and vacillating breathing (or swinging), have been extensively studied. Understanding of these dynamics has helped give more insight into rheology of dilute vesicle [27,31,32] and capsule suspensions [33,34].

However, in physiological conditions, blood is highly concentrated, with an average hematocrit of 45% in the human body (in microcirculation, the hematocrit is lower, in the range of 10–20% [35]). Thus, hydrodynamic interaction among RBCs, as well as the presence of bounding walls, should be taken into account for a better description of situations which are relevant to blood flow [27,36]. Semidilute and concentrated suspensions exhibit a diffusion-like process leading to a mixing of cells [37–39], as well as a formation of a depletion layer (cell-free layer) near vessel walls in a pressure-driven flow. As a first fundamental question of the collective dynamics, the interaction between two bodies in simple flow has been considered by several groups [40–43]. For example, a lateral shift (orthogonal to the flow direction) in trajectories of the particles is observed after they pass each other in the shear flow, which results in the so-called shear-induced diffusion.

The study of blood rheology in unconfined configurations was of considerable interest in the past [44,45]. However, the confined geometries have been less studied so far. Recently, several studies have revealed that the confinement can have a significant influence on the dynamics of a single deformable particle [46,47] as well as on the rheology of a suspension of vesicles [48–51] in simple shear flow. Drastic effects are also reported for suspensions of confined rigid particles [52–54].

The goal of this study is to advance the understanding of the basic hydrodynamical mechanisms that govern the rheology of suspensions in confined geometry, in application to blood rheology. Since this topic is largely unexplored, our aim is not to tackle complex situations by including all suspected ingredients, but rather to focus on a simplified model system with the hope of elucidating basic phenomena. For this purpose, we simplify the problem by considering a suspension of vesicles and leave the modeling of RBC mechanics to other studies. Furthermore, we focus our study on a two-dimensional (2D) model. Our recent work has pointed out [51] that when it comes to the rheology and spatial organization (in the form of a chain of RBCs), the simplified model of a 2D suspension of vesicles leads to the same basic conclusion as the full three-dimensional (3D) model of RBC suspension. However, whether the 3D suspension can reveal the formation of a crystalline structure is an open question. We will here take advantage of the low numerical cost of 2D simulations in order to study more systematically the rheology of a confined suspension of vesicles. The systematic 3D study will be considered in the future.

We consider a linear shear flow, which provides the simplest form of hydrodynamic forcing for a confined suspension. The results of this study are thus relevant to *in vitro* measurements of blood viscosity. Another potential application is the design of microfluidic devices, for example, for the diagnosis of blood-related diseases: Several diseases, such as sickle-cell anemia, are as characterized by an increased stiffness of the RBCs. Our results show that the mechanical properties of the particles, such as their viscosity contrast, affect the ordering of the suspension, which has a strong rheological signature. This can serve as a simple diagnostic tool of blood pathologies. Blood flow *in vivo* occurs in vessels and is of Poiseuille type. This makes it difficult to apply the present study to *in vivo* situations. Nevertheless, some phenomena observed in a linear shear flow are also expected to manifest themselves in a pressure-driven flow because blood flow close to vessel walls can be approximated as a linear shear flow.

This paper is a followup of a recent brief report [51]. Here, besides providing an extended discussion, we present several interesting aspects: (i) the flow field created by a vesicle is analyzed under close scrutiny and this provides a clear image of the existence of a stationary state of two confined and tank-treading vesicles. This stationary state is shown to play a key role in the spatial organization. (ii) We analyze the role of a viscosity contrast and show that even vesicles with very viscous internal fluid can organize into a regular pattern if confinement is strong enough to induce tank treading, while for weaker confinements, disorder prevails and the vesicles show tumbling. (iii) We provide a link between spatial organization and the rheological features of the suspension, showing that the normalized viscosity as a function of concentration either shows a nonmonotonic behavior for ordered suspensions or a monotonic behavior (associated with disorder). We find that the total effective viscosity exhibits plateaus as a function of concentration, which we attribute to the appearance of order. In some small intervals of concentration, we observe that even the total viscosity of the suspension decreases with increasing concentration.

This paper is organized as follows. In Sec. II, we present the method and the model equations. Section III is dedicated to the validation of the method where we compare the lattice Boltzmann method (LBM) with the boundary integral method (BIM). In Sec. IV, we present and analyze the main results of this paper. Section V sums up the results and provides some perspectives.

II. MODEL AND NUMERICAL METHOD

A. Model

The present work is based on simulations of 2D model vesicles by using the lattice Boltzmann method (LBM) of solving fluid dynamics equations coupled with the immersed boundary (IB) method for modeling fluid-structure interactions. These methods possess many desirable properties, such as computational efficiency for suspensions of multiple deformable particles, ease of implementation, and decent precision. In our recent study [51], most of the results were obtained in 2D by using the boundary integral method (BIM), whereas IB-LBM was reserved for 3D simulations. Here we validate our implementation of IB-LBM by comparing its results with BIM for several test problems.

The 2D simplification used here assumes the system to be translationally invariant along one dimension, which we here choose to coincide with the z axis. With this assumption, the full 3D behavior of the system can be deduced from the 2D dynamics in the x,y plane. The fluid dynamics inside or outside the vesicles is governed by the Navier-Stokes equations

$$\nabla \cdot \mathbf{u} = 0, \tag{1}$$

$$\rho\left(\frac{\partial \mathbf{u}}{\partial t} + \mathbf{u}\cdot\nabla\mathbf{u}\right) = -\nabla p + \eta_{\{\text{ext,int}\}}\nabla^2\mathbf{u} + \mathbf{F}, \tag{2}$$

where $\mathbf{u}$ is the fluid velocity, ρ is the fluid density, and η is the fluid viscosity, which we set equal to η_{int} or η_{ext} inside and outside of the vesicles, respectively. The force $\mathbf{F}$ is applied to the fluid by the vesicles. A dimensionless parameter $\lambda = \eta_{\text{int}}/\eta_{\text{ext}}$ is called viscosity contrast. Several values of λ are explored in this study but the emphasis is made on two extreme values, 1 and 10, which lead to tank-treading and tumbling motion, respectively, for weakly confined vesicles (tumbling may be suppressed in favor of tank treading for sufficiently strong confinement).

Equations (1) and (2) are solved with boundary conditions

$$u_x(X,\pm W/2) = \pm\dot{\gamma}W/2, \quad u_y(X,\pm W/2) = 0, \tag{3}$$

where X and Y (used below) are the x and y components of the position vector, respectively, W is the distance between the walls, and $\dot{\gamma}$ is the shear rate. $Y = -W/2$ and $Y = W/2$ correspond, respectively, to the lower and upper walls of the channel. Equations (1) and (2) together with the boundary conditions (3) impose a simple shear flow with shear rate $\dot{\gamma}$ for a simple Newtonian fluid.

The vesicles are represented by closed one-dimensional (1D) contours, which result from a cross section of the vesicle membranes by the x,y plane. The no-slip boundary conditions at the membrane imply that the contours are advected with the velocity of the immediately adjacent fluid. The integral properties of the vesicles, namely surface area, volume, and elastic energy, have to be measured per length unit along the z direction. Consequently, the surface area and the inner volume of the vesicle are quantified by, respectively, the length L and the enclosed area s of the contour in the 2D model. We define the reduced area (2D analog of the reduced volume) as $\nu = 4\pi s/L^2$, where L is the vesicle perimeter. For a circle, we have $\nu = 1$, whereas $\nu < 1$ for any other shapes. In this study, we have mainly explored the case $\nu = 0.7$ that provides a biconcave equilibrium shape, although other values have also been tested as reported below.

The resistance of vesicles to deformations is governed by their elastic energy E, which accounts for the inextensibility of the membrane and the bending energy,

$$E = \oint_L \zeta dL + \frac{1}{2}\kappa \oint_L C^2 dL, \tag{4}$$

where ζ is a position-dependent Lagrange multiplier that ensures the inextensibility of the membrane, κ is the 3D bending modulus, and C is the local curvature of the contour. The integration in Eq. (4) is taken along the vesicle contour in the 2D model, with dL being the element of arc length on the contour. As discussed above, the energy (4) is measured per unit length in the z direction. The membrane force $\boldsymbol{f}$ is calculated as a variational derivative of the energy (4), according to the following expression in 2D:

$$\delta E = -\oint_L \boldsymbol{f} \cdot \boldsymbol{\delta r} dL, \tag{5}$$

where δE is the variation of energy (4) upon the infinitesimal deformation $\boldsymbol{\delta r}$ of the vesicle contour. The force density $\boldsymbol{F}$ in Eq. (2) is related to $\boldsymbol{f}$ in Eq. (5) by the following relation:

$$\boldsymbol{F}(\boldsymbol{r}_f) = \oint_L \boldsymbol{f}(\boldsymbol{r}_m)\delta^{2D}(\boldsymbol{r}_f - \boldsymbol{r}_m)dL(\boldsymbol{r}_m), \tag{6}$$

where $\boldsymbol{r}_f$ is a given point in the fluid domain and $\boldsymbol{r}_m$ is a point on the membrane. Here δ^{2D} is the 2D Dirac δ function, as required by the 2D model. The ratio of the viscous stresses due to the imposed flow and the elastic stresses due to vesicle deformation can be characterized by defining a capillary number C_a as

$$C_a = \frac{\eta_{\text{ext}} R^3 \dot{\gamma}}{\kappa}, \tag{7}$$

where $R = \sqrt{s/\pi}$ is the characteristic size of the vesicle. C_a is set to 1 in most of our simulations, but we have also explored other values of C_a (0.1 and 10) without noticing a significant change of our results, as discussed below.

The set of equations (1)–(6) allows one to calculate the velocity everywhere in the fluid domain for a given conformation of vesicles and a given distribution of the Lagrange multiplier ζ, which provides also the velocity at the vesicle contours. The system is closed by imposing the membrane inextensibility condition, which can be solved for the Lagrange multiplier ζ. We treat the above model numerically using the IB-LBM.

B. Numerical method

First, we briefly recall for completeness the main steps of the LBM (see Refs. [55–57] for details). In LBM, a fluid is treated as a cluster of pseudofluid particles. They collide and spread along discrete directions at each spatial position. The distribution function $f_i(\mathbf{r},t)$, the main quantity in LBM, gives the probability of finding a particle having lattice velocity $\mathbf{c}_i$ at position $\mathbf{r}$ at time t. The so-called D2Q9 lattice model (9 lattice velocity vectors in 2D) is employed in order to guarantee the isotropy of the fluid. The time evolution of the distribution function $f_i(\mathbf{r},t)$ is governed by the lattice Boltzmann equation:

$$f_i(\mathbf{r} + \mathbf{c}_i \Delta t, t + \Delta t) - f_i(\mathbf{r},t) = \Omega_i + \Delta t F_i, \tag{8}$$

where Δt is the time step and F_i is a bulk force term to be specified below. Here Ω_i is the collision operator, for which the Bhatnagar-Gross-Krook (BGK) approximation is often adopted:

$$\Omega_i = -\frac{1}{\tau}\left[f_i(\mathbf{r},t) - f_i^{eq}(\mathbf{r},t)\right], \tag{9}$$

where τ is a dimensionless relaxation time, related to the kinematic viscosity of the fluid $\upsilon = \frac{1}{2}c_s^2 \Delta t(2\tau - 1)$. Here

$$c_s = \frac{1}{\sqrt{3}}\frac{\Delta x}{\Delta t} \tag{10}$$

is the speed of sound in lattice units for the D2Q9 model. In this paper, we set $\Delta x = 1$ and $\Delta t = 1$ in the LBM units. The viscosity η of the fluid can be varied in the LBM by adopting two different relaxation times inside and outside the vesicles in the BGK expression (see Ref. [58] for the implementation of a viscosity contrast). In our simulations, we set $\tau = 1$, yielding $\upsilon = 1/6$ for the viscosity in the LBM units. Then a viscosity contrast is created thanks to a different choice of τ for the fluid inside the vesicle. For example, for viscosity contrast $\lambda = 10$ we set $\tau = 5.5$ for the fluid inside the vesicle.

The equilibrium distribution f_i^{eq} is obtained from an approximation of the Maxwell distribution and can be expressed as

$$f_i^{eq} = \omega_i \rho \left[1 + \frac{1}{c_s^2}(\mathbf{c}_i \cdot \mathbf{u}) + \frac{1}{2c_s^4}(\mathbf{c}_i \cdot \mathbf{u})^2 - \frac{1}{2c_s^2}(\mathbf{u} \cdot \mathbf{u}) \right]. \tag{11}$$

Here F_i is the bulk force term, which can be written as [59]

$$F_i = \left(1 - \frac{1}{2\tau}\right) \omega_i \left(\frac{\mathbf{c}_i - \mathbf{u}}{c_s^2} + \frac{\mathbf{c}_i \cdot \mathbf{u}}{c_s^4} \mathbf{c}_i \right) \cdot \mathbf{F}, \tag{12}$$

where $\mathbf{F}$ is the force density. For the D2Q9 model, the nine lattice velocities $\mathbf{c}_i$ and weight factors ω_i are $\mathbf{c}_i = (0,0)$, $\omega_i = 4/9$ for $i = 0$; $\mathbf{c}_i = (\cos[i-1]\pi/2, \sin[i-1]\pi/2)\Delta x/\Delta t$, $\omega_i = 1/9$ for $i = 1,2,3,4$; and $\mathbf{c}_i = (\cos[2i-9]\pi/2, \sin[2i-9]\pi/2)\Delta x/\Delta t$, $\omega_i = 1/36$ for $i = 5,6,7,8$.

The macroscopic quantities can be expressed once the distribution function f_i is determined from Eq. (8). The fluid density is given by

$$\rho = \sum_i f_i. \tag{13}$$

The fluid velocity is obtained as [59]

$$\rho \mathbf{u} = \sum_i \mathbf{c}_i f_i + \frac{1}{2} \Delta t \mathbf{F}. \tag{14}$$

The fluid pressure follows from the relation $p = c_s^2 \rho$ (local equation of state). In the limit of small Mach and Knudsen numbers, it has been shown, through the Chapman-Enskog expansion, that the lattice Boltzmann equation recovers the incompressible Navier-Stokes equations (1) and (2) [55].

A vesicle contour is represented by N membrane points. In most of our simulations, we set $N = 150$. Each membrane point is connected to its two neighbors with the potential [60,61]

$$E_l = \frac{1}{2} k_l \sum_{i=1}^{N} \left(\frac{l_i - l_0}{l_0} \right)^2, \tag{15}$$

where k_l is a springlike constant, which is set as large as possible (0.2 in the LBM units in our simulations) in order to keep the perimeter of the membrane constant. l_i is the actual spring length and l_0 is the equilibrium spring length. Equation (15) replaces the strictly inextensible membrane in Eq. (4) by a weakly extensible one, whose dilatation is strongly penalized by large spring constants k_l. This effectively removes the need to solve a large linear system in order to calculate the Lagrange multiplier ζ at each membrane point at the price of small deviation of the membrane perimeter from the prescribed value. A similar penalization technique has been adopted in previous studies on continuum models of 2D vesicles [32,62]. To maintain the area s of the internal fluid of the vesicle at a constant value s_0, we adopt an additional penalization term in the potential energy [60,61]

$$E_s = \frac{1}{2} k_s \left(\frac{s - s_0}{s_0} \right)^2, \tag{16}$$

where k_s is a constant chosen as large as possible in order to guarantee a constant enclosed area. Setting $k_s = 1000 k_l$ in the simulations reduces the area changes to small fluctuations (less than 1%).

The fact that k_s is significantly higher than k_l can be partially understood by noting that Eq. (15) has N terms, while there is only a single term in Eq. (16). Thus Nk_l should be comparable with k_s. It turns out that about $k_s \sim 6Nk_l \sim 1000k_l$ is required in order to ensure the conservation of the enclosed area of the vesicles. The value of l_0 is set to 0.62 in the LBM grid units. l_0 approximately represents the Lagrangian mesh size, which is ideally chosen around half of the Eulerian grid in the IB method to avoid numerical "stick" and "leakage". To account for the fixed reduced area, we also need to satisfy a relationship between l_0 and s_0 given by $4\pi s_0/(Nl_0)^2 = \nu$.

The bending energy in Eq. (4) is modeled as [60,61]

$$E_b = \frac{1}{2}k_b \sum_{i=1}^{N} \tan^2\left(\frac{\theta_i}{2}\right), \tag{17}$$

where k_b is the bending constant and θ_i is the supplementary angle between two springs connected to the membrane point i. It is easy to establish a relation between the bending modulus κ in Eq. (4) and the bending constant k_b in Eq. (17) by considering a circle of radius R_C. The bending part of the energy (4) is equal to $\kappa\pi/R_C$, in this case, while Eq. (17) gives $E_b = \frac{1}{4}k_b l_0 \pi/R_C$. This yields a relationship between k_b and κ, which reads

$$\kappa = \tfrac{1}{4}k_b l_0. \tag{18}$$

The membrane force on each point at each time step is calculated from the potentials (15)–(17) by taking the derivative

$$\mathbf{F} = -\frac{\partial(E_l + E_b + E_s)}{\partial \mathbf{r}}. \tag{19}$$

This force is coupled to the LBM solver of the fluid flow by using the IB method [46,57,63]. This method was developed originally by Peskin and has been proven very useful for simulating flexible membranes in fluid flows [64]. The basic idea is, on the one hand, to spread the force defined at membrane points (which are off lattice) to nearby fluid points (which are on lattice) and, on the other hand, to interpolate the velocity from the nearby fluid points to the membrane. The IB method does not treat the membrane as a sharp interface but as a band where the membrane forces are distributed thanks to a smeared δ function. Thus, the presence of the membrane is characterized by a bulk force (the force in the band), which enters the right hand side of the Navier-Stokes equations. The fluid-structure interaction is materialized thanks to these bulk forces representing the membrane and entering the Navier-Stokes equations.

The membrane force is spread out thanks to a smeared δ function D^{2D} (to be defined below), which substitutes the exact δ function δ^{2D} in Eq. (6) as

$$\mathbf{F}(\mathbf{r}_f) = \sum_m D^{2D}(\mathbf{r}_f - \mathbf{r}_m)\mathbf{F}(\mathbf{r}_m). \tag{20}$$

Similarly we interpolate the fluid velocity from the lattice toward the membrane points by using

$$\mathbf{u}(\mathbf{r}_m) = \sum_f D^{2D}(\mathbf{r}_m - \mathbf{r}_f)\mathbf{u}(\mathbf{r}_f). \tag{21}$$

The new position of the membrane is obtained by displacing each point on the membrane by an amount given by the product of this velocity with a time step.

Usually, the smeared δ function is taken to have the following property:

$$D^{2D}(\mathbf{r}) = \phi(r_x)\phi(r_y). \tag{22}$$

The choice of the function ϕ is based on a smoothed three-point discrete δ function [65]:

$$\phi(r) = \begin{cases} \frac{17}{48} + \frac{\sqrt{3}\pi}{108} + \frac{|r|}{4} - \frac{r^2}{4} + \frac{1-2|r|}{16}\sqrt{-12r^2+12|r|+1} - \frac{\sqrt{3}}{12}\arcsin\left(\sqrt{3}|r| - \frac{\sqrt{3}}{2}\right) & |r| \leqslant 1 \\ \frac{55}{48} - \frac{\sqrt{3}\pi}{108} - \frac{13|r|}{12} + \frac{r^2}{4} + \frac{2|r|-3}{48}\sqrt{-12r^2+36|r|-23} + \frac{\sqrt{3}}{36}\arcsin\left(\sqrt{3}|r| - \frac{3\sqrt{3}}{2}\right) & 1<|r|<2, \\ 0 & |r| \geqslant 2 \end{cases} \tag{23}$$

where r is expressed in the LBM units.

A numerical contact between a vesicle and another vesicle or a wall can occur in the course of simulation. A straightforward way to avoid this contact is to refine the resolution of the domain. However, this comes at a price: The computational time would increase dramatically. As a more practical solution, a repulsive force is added in our simulations in order to keep the distance between two interfaces larger than the interpolation range. This force is introduced thanks to a Morse potential [66],

$$\Phi(d) = \begin{cases} D_e[e^{2\beta(d_0-d)} - 2e^{\beta(d_0-d)}] & d \leqslant d_0 \\ 0 & d > d_0 \end{cases}, \tag{24}$$

where the parameters D_e and β have the value of 0.0001 and 2 in the LBM units, d is the distance between two membrane points, and d_0 denotes the repulsion range, set to two lattice lengths in the simulations. We must mention that the numerical collision can, in principle, be avoided thanks to this repulsion. However, this is not always obvious. One drawback is that the real effective radius of the vesicle is made artificially larger (due to the smeared δ function), and this might be a source of errors, especially for highly concentrated suspensions. The question of how this problem can be fully circumvented without resorting to *ad hoc* rules is a matter of ongoing debate in the literature. We have tested IB-LBM results against the BIM, as discussed below, a fact that validates, to some extent, our method.

We report below the effective viscosity of the suspension. It is defined as $\eta = \langle\sigma_{xy}\rangle/\dot{\gamma}$, where σ_{xy} is the wall shear stress. The symbol $\langle\cdots\rangle$ designates here a double average over the bounding wall and over time. The shear stress tensor σ_{xy} in LBM can be expressed in terms of the distribution function as [67]

$$\sigma_{xy} = -\left(1 - \frac{1}{2\tau}\right)\sum_i c_{ix}c_{iy}\left(f_i - f_i^{eq}\right), \tag{25}$$

where c_{ix} and c_{iy} are the x and y components of lattice velocity $\mathbf{c}_i$ respectively.

III. VALIDATION

To validate our method, we compare the results obtained with IB-LBM to those obtained by BIM for several test cases. In BIM, a continuum model is used to represent the vesicle and discretize the elastic energy (4). The BIM couples the membrane force to the fluid flow through an integral equation. The integral equation is obtained using the Green's function technique applied to the Stokes equations, which correspond to the limit $\rho \to 0$ of Eqs. (1) and (2) [50].

We simulate a single vesicle in linear shear flow with two bounding walls as shown in Fig. 1(a). In these tests, the computational domain is $60R \times W$ with periodic boundary conditions along the x direction. R is chosen as $12\Delta x$ for the resolution in IB-LBM. Two values of W ($5R$ and $16R$) are used for the examination of tank treading and tumbling motions respectively. The membrane is represented by $N = 150$ nodes in IB-LBM, while 128 nodes are used for the membrane in BIM. We set the Reynolds number as $\mathrm{Re} = \rho R^2\dot{\gamma}/\eta_{\mathrm{ext}} = 0.002$ in IB-LBM, which is small enough to satisfy the stokes limit ($\mathrm{Re} = 0$). The capillary number C_a is fixed to 1 and the reduced area is set to 0.7 in the validation tests.

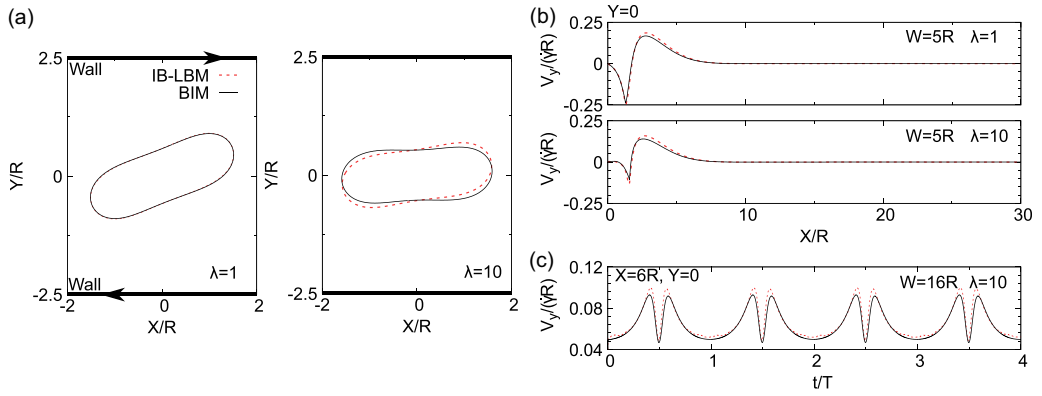

FIG. 1. Comparison between IB-LBM and BIM. (a) The shape of a tank-treading vesicle in the case of $W = 5R$. (b) The y component of the velocity field at the center of the channel ($W = 5R$). (c) The time evolution of y component of the velocity field at a given point located at (6R,0) in the case of $W = 16R$. Time is rescaled by the tumbling period T, which is found to be equal to $14.5\dot{\gamma}^{-1}$ for the IB-LBM and $12.4\dot{\gamma}^{-1}$ for the BIM.

In Fig. 1(a), we show the shape of a tank-treading vesicle and its orientation with respect to the flow direction. We do not observe any noticeable difference between IB-LBM and BIM for $\lambda = 1$. However, for $\lambda = 10$, the inclination angle in IB-LBM is slightly larger than that in BIM. This deviation is also reported in Ref. [58]. The reason is attributed to residual inertial effects. Another possible source of error can stem from the algorithm implementing the viscosity contrast. Indeed, a value of τ larger than 1 is known to affect the quality of the numerical results [68]. Figure 1(b) shows the y component of the velocity field in the middle of the channel in the case of $W = 5R$. A good agreement between LBM and BIM is achieved. Figure 1(c) displays the evolution of the y component of the velocity field at a given arbitrary point with coordinate ($6R$,0) as a function of time for the case of $W = 16R$, in which the vesicle exhibits tumbling motion. The velocity obtained by IB-LBM exhibits the same overall features of flow field produced by a tumbling vesicle, though it shows a slightly longer period of oscillation compared to the BIM.

Finally, we report the grid convergence in Fig. 2. We consider the same case treated in Fig. 1(a), but with a higher Reynolds number 0.2, which is used in most of our simulations, providing a quite

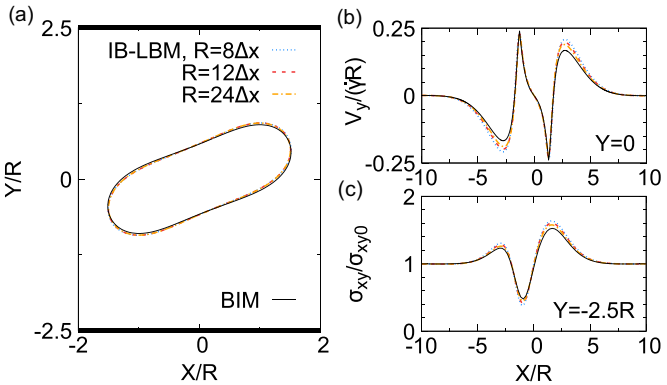

FIG. 2. Grid convergence. (a) The shape of a tank-treading vesicle. (b) The y component of the velocity field in the center of the channel. (c) The shear stress along the bottom wall in the presence of the vesicle σ_{xy}, normalized by the shear stress in the absence of the vesicle σ_{xy0}.

reasonable agreement with the BIM (though occasionally we used a much smaller value of Re in order to test the sensitivity of our results to inertia). Three resolutions ($R = 8\Delta x$, $R = 12\Delta x$, and $R = 24\Delta x$) are considered. The results show a quite good grid convergence as presented in Fig. 2, where we report the shape of a tank-treading vesicle, the y component of the velocity field at the channel center, and the shear stress at the bottom wall.

IV. RESULTS

In this study, we consider a suspension of vesicles sheared between two countermoving rigid plane walls, which are located at $Y = -W/2$ and $Y = W/2$. Periodic boundary conditions are applied at the two lateral boundaries which are orthogonal to the flow direction. The length of the computational domain along the flow direction is fixed to $63.7R$ (800 grid points), with $R = 12.55$ in the LBM units for the resolution, while the gap is varied in some wide range, to be specified below. The Reynolds number is set to 0.2. Vesicles in 2D exhibit two types of motion, (i) tank treading and (ii) tumbling, depending on viscosity contrast and confinement. The former motion is characterized by stationary shape and orientation of the vesicle, while the latter one corresponds to a periodic rotation of the direction of the longest axis of the vesicle. We examine two extreme values of the viscosity contrast: $\lambda = 1$, which always leads to tank-treading of vesicles, and $\lambda = 10$, which may lead to either tumbling (weak confinement) or tank treading (strong confinement). We show that the overall dynamical and rheological features of the suspension depend mainly on whether the vesicles exhibit tank treading or tumbling, and the precise value of λ does not matter on the qualitative and even on the quantitative level in many cases. As a test, we examine an intermediate value $\lambda = 5$ in order to show that the equilibrium distance between two vesicles, whenever it exists, is practically unaffected by the value of λ.

A. Interaction between two tank-treading vesicles

The interaction between two tank-treading vesicles in unbounded shear flow has been investigated by several groups [40–43]. When two vesicles move towards each other along the flow direction and pass each other, their mutual hydrodynamic interaction induces a lateral migration along the velocity gradient direction, that pushes them away from each other. This interaction plays an important role in the shear-induced diffusion of suspensions of deformable particles. In the absense of bounding walls, the lateral separation of the two vesicles tends to a final steady-state value after they pass each other. However, different behavior is observed in confined suspensions: When the flow is confined between two walls, a lateral migration of the vesicle is caused by the lift from a given wall, which tends to push the vesicle towards the centerline. Due to symmetry, both walls have opposite effects and one expects the vesicle to stop at the centerline (this expectation may be violated if the shape of the vesicle undergoes a parity-symmetry-breaking, discovered in Ref. [69]). Consequently, two vesicles that pass near each other in confined shear flow have a tendency to return to the centerline of the channel unless they are disturbed by other vesicles in the suspension.

For all explored situations, we find that a single vesicle always settles into the flow centerline. Additionally, we find that two vesicles always keep, after some transience, a constant interdistance ΔX (which we define as the difference between the x components of the centers of mass of the membranes of the two vesicles) when they reach the centerline. As shown in Fig. 3, starting from different initial positions, the pair of vesicles always reaches the same terminal interdistance. In most of the present simulations, the initial shape of the vesicles is the equilibrium shape obtained in quiescent fluid. We have also explored several other initial configurations (such as an elliptical shape) and have found no difference regarding the final state. The robustness of the results with respect to the length of the simulation box has been checked systematically. As a way of example, the same results are obtained by using double size of the current box.

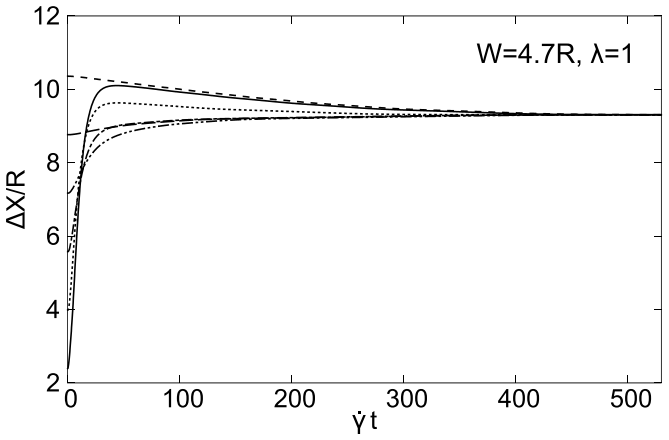

FIG. 3. The interdistance between two tank-treading vesicles as a function of time. Different curves show cases of different initial positions. All the cases finally reach an equilibrium state with constant interdistance.

1. Analysis of the flow field created by a single confined vesicle

In order to dig into the mechanisms which cause the appearance of a bound state in the presence of confinement, the velocity field created by a single confined vesicle is analyzed first. We focus on the induced flow, which is nothing but the total flow minus the imposed linear shear flow. The result is presented in Fig. 4 for a vesicle performing tank-treading motion. We first notice the presence of vortices in the form of a quadrupole-like pattern surrounding the vesicle. This recirculation is a direct consequence of confinement. Let us focus on the region located on the right side away from the vesicle (Fig. 4, middle and bottom). There is an anticlockwise recirculation with the flow field pointing upward in the immediate vicinity of the vesicle. Streamlines in this area ascend, deflect from the upper wall, bounce backward, and form a second recirculation farther to the right, a clockwise vortex as shown in Fig. 4. This flow pattern becomes more pronounced upon increasing confinement.

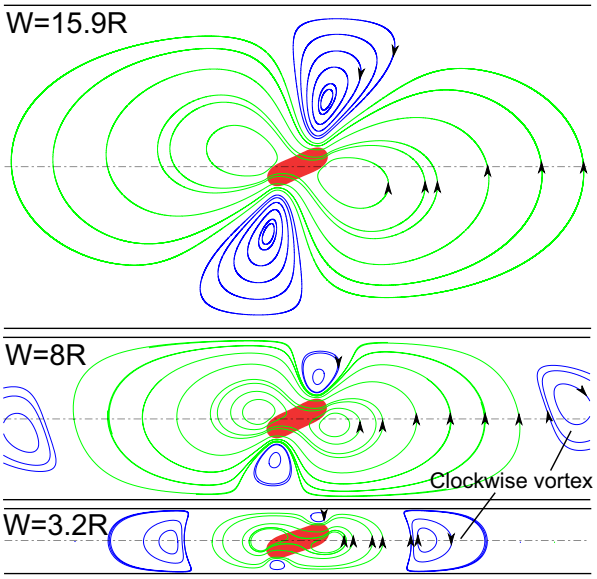

FIG. 4. The structure of the induced flow for different confinements.

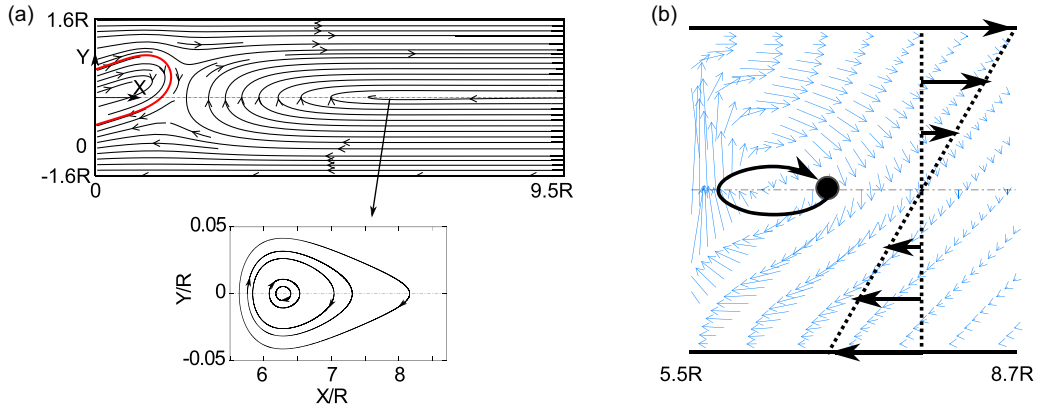

FIG. 5. (a) The streamlines of flow field around a single tank-treading vesicle (only a subdomain from 0 to $9.5R$ is presented). We also show an enlargement of the region where the flow field shows a stagnation point. (b) The flow lines corresponding to the induced flow in the region from $5.5R$ to $8.7R$ and a schematic of the motion of a tracer.

The clockwise vortex is closer to the vesicle when W decreases. This clockwise vortex constitutes the key element for the formation of an equilibrium state made of two vesicles. Indeed, and as is shown below, this clockwise vortex constitutes a stagnation point for tracers.

First, let us analyze the motion of a tracer. In Fig. 5, we show the flow field obtained for $W = 3.2R$ and analyze the behavior of a tracer located in the region of the clockwise vortex. The tracer is initially placed at centerline. The schematic of tracer trajectory is shown in Fig. 5(b). Only in the region having a clockwise vortex does the trapping of the tracer take place.

2. *Vesicle-vesicle interaction*

If a tracer is substituted by a vesicle, one is tempted to expect a qualitatively similar scenario, though a vesicle cannot be viewed as a tracer, since it perturbs the flow field around it. However, we may consider the reasoning above as a crude vision of the possible existence of a bound state between the two vesicles. When the second inserted vesicle is located within the clockwise vortex region, like the tracer in Fig. 5(b), its center of mass has a tendency to follow a closed trajectory (as does the tracer). However, due to the finite extent of the vesicle (in contrast to a pure tracer) it is always pushed toward the center of the channel, thanks to the wall-induced lift force. This means that the trajectory of the center of mass quickly decays and settles into the centerline. This is expected to lead to a stationary configuration of two vesicles.

In order to lend further support to the above result, we have performed the following analysis. We first take a single vesicle and compute the distance at which the Y component of the velocity changes sign in the centerline ($Y = 0$) and denote it as X^*. X^* approximately gives the position of the center of the clockwise vortex. Figure 6 presents the results for different confinements, showing that X^* depends, approximately, linearly on W. The next step consists in taking a pair of vesicles and finding the final equilibrium interdistance. Interestingly, it is found that this interdistance is very close to X^* (Fig. 7).

A systematic study is then undertaken in order to analyze the behavior of a pair of vesicles in a confined shear flow. We have explored several values of confinement, capillary number, reduced area, and viscosity contrast. All simulations have confirmed the tendency discussed above, in that the presence of a clockwise vortex is the source of the formation of a bound state of the pair of vesicles. The results are summarized in Fig. 7. We find a linear relationship between the equilibrium interdistance of a pair and the confinement. We compare systematically this distance to that denoted above as X^* (center of the clockwise vortex created by a single vesicle). The two results show a

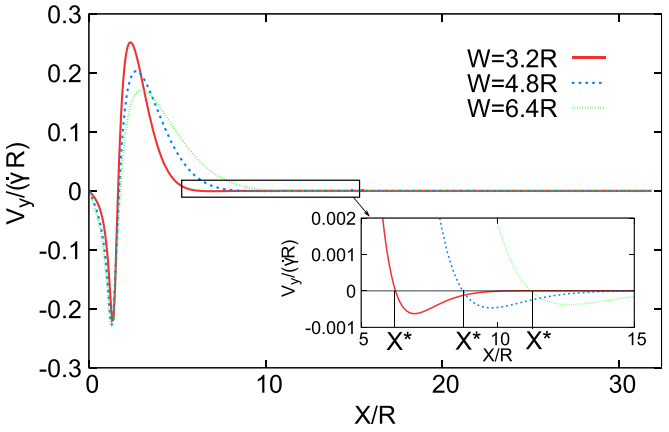

FIG. 6. V_y as a function of X along the centerline for different confinements. The inset is an enlarged region corresponding to the clockwise vortex. The central position of the vortex is denoted as X^*.

good agreement [Fig. 7(a)]. This result highlights the fact that the simple reasoning based on the analysis of the velocity field due to a single vesicle already captures the essential features of the pair dynamics. This observation is interesting inasmuch as it offers a simplified basis for future analytical calculations where only a single vesicle can be taken into account in order to draw general

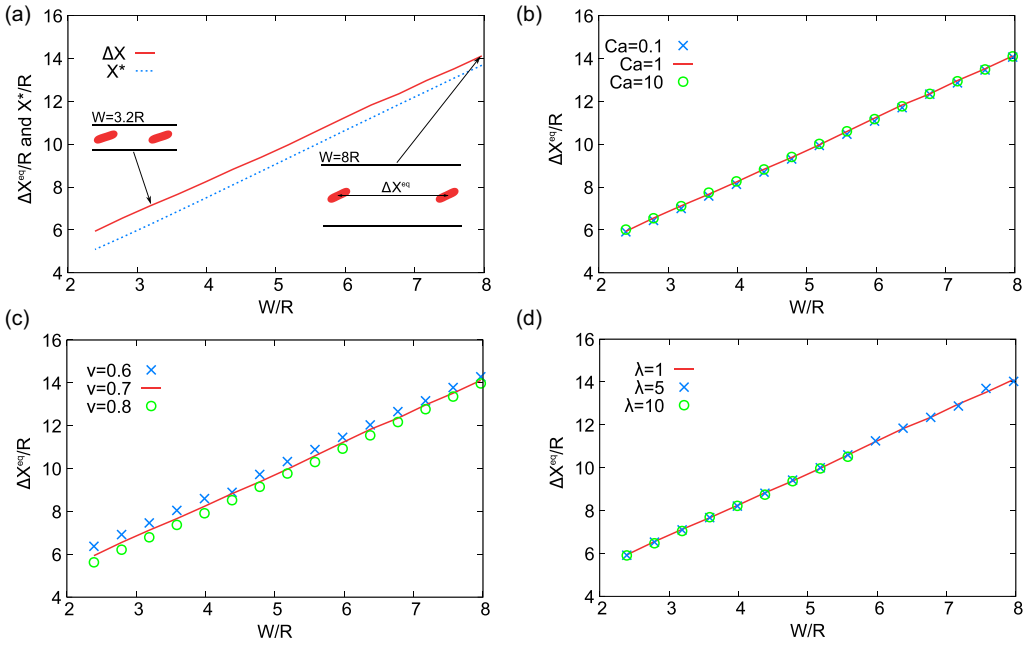

FIG. 7. The equilibrium interdistance between two vesicles increases quasilinearly with W. (a) The insets show the finial spatial configurations of the vesicles in the cases of $W = 3.2R$ and $W = 8R$. The dashed line shows X^* as a function of confinement. The solid line shows the distance between the vesicles as a function of confinement. (b) Interdistance as a function of confinement for different capillary numbers. (c) Interdistance as a function of confinement for different reduced area. (d) Interdistance as a function of confinement for different viscosity contrasts.

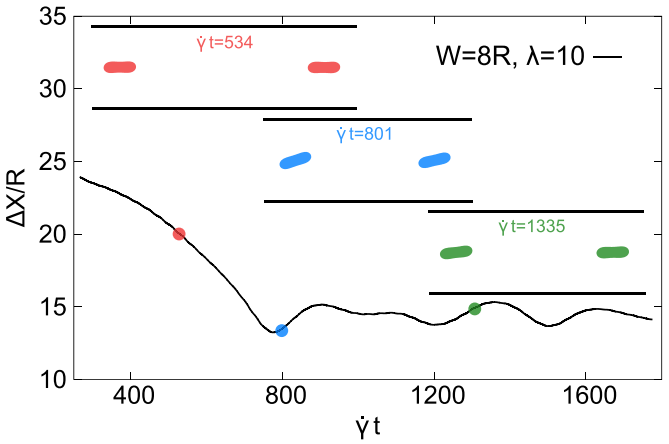

FIG. 8. The interdistance between two tumbling vesicles as a function of time. The insets are the configurations of the vesicles at the time of $\dot{\gamma}t = 534$, $\dot{\gamma}t = 801$, and $\dot{\gamma}t = 1335$.

conclusions on the behavior of pairs of vesicles (or even a collection of vesicles) in a channel. We also found that the capillary number, the reduced area, and the viscosity contrast have minor effects on this linear relationship as shown by Figs. 7(b)–7(d). Note that for $\lambda = 10$ we do not include the cases with $W > 6R$ since the vesicles perform a tumbling motion in this regime which does not lead to a final stationary interdistance of the pair, as explained below.

Finally, let us make few remarks on the linear behavior of the equilibrium interdistance with the channel gap W. By fitting the data, we get $\Delta X^{eq} = 1.47W + 2.42R$, where ΔX^{eq} denotes the equilibrium interdistance. This behavior can be understood as follows. When W increases, a fluid particle (or a tracer) deflected by a vesicle travels a longer distance before bouncing back on the wall. The angle of deflection after impact on a vesicle is expected to be rather insensitive to W, so that the distance traveled by a tracer before it bounces back increases linearly with W. Thus, we expect the location of the stagnation point (the center of the clockwise vortex in Fig. 4) to scale as W.

B. Interaction between two tumbling vesicles

Besides tank treading, vesicles are known to exhibit tumbling for a sufficiently large viscosity contrast λ. A tumbling vesicle creates an oscillating in time flow pattern as shown in Fig. 1(c). From this flow, we infer that a tracer located at some distance from the tumbling vesicle would oscillate both vertically and horizontally in time and exhibit an apparently erratic trajectory. In principle, another vesicle located nearby would oscillate irregularly in time.

The interdistance between two vesicles for the tumbling case are presented in Fig. 8. Figure 8 shows the distance along the flow direction between the centers of mass of two tumbling vesicles as a function of time. While the pair of vesicles remain at some interdistance on the average, the instantaneous interdistance varies with time in an irregular fashion. We cannot talk of an equilibrium state in the same sense as we did for tank-treading vesicles. We thus do not expect a suspension of tumbling vesicles to exhibit any kind of order, a question which is discussed further below.

C. Spatiotemporal organization of a vesicle suspension

Based on the understanding of the interaction between two vesicles, we hope to extract some general conclusions on the overall flow behavior of a suspension containing many vesicles. We would like to see how confinement influences the configuration of a vesicle suspension. We have

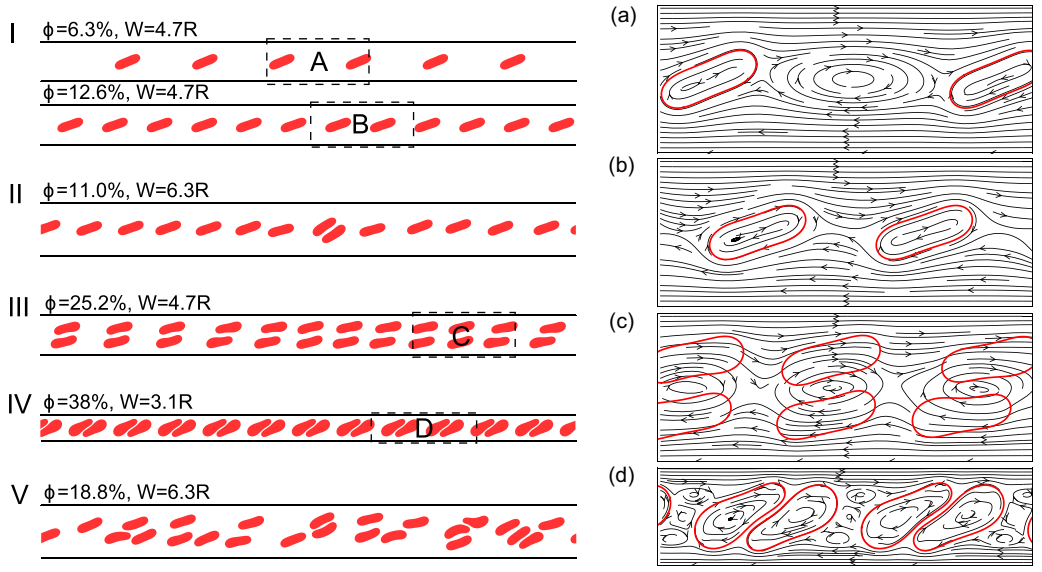

FIG. 9. Left panel: Configurations of suspension for pattern I (one-file solution), pattern II (transition region which precedes one-file to two-file solutions and shows several structural defects), pattern III (two-file solution), pattern IV (doublets), and pattern V (disorder). Right panel: The structure of the flow field in regions A, B, C, and D.

systematically analyzed this question by exploring concentrations from 0 to 40% for three different confinements: $W = 3.1R$, $4.7R$, and $6.3R$.

First, we consider the case with $\lambda = 1$. As we have reported in Ref. [51], several configurations of vesicle suspension are observed. Various patterns are shown in Fig. 9. A systematic analysis has allowed us to draw the phase diagram of several ordering patterns (Fig. 10). The spatial configurations of the suspension corresponding to each ordered pattern can be read in Fig. 9. Starting from an initial configuration of the suspension chosen randomly within the channel, vesicles first experience a lift force due to the walls. Because of symmetry, the vesicles settle at the centerline exhibiting a one-file structure (an ordered alignment; see pattern I in Fig. 9) in the case of a sufficiently dilute

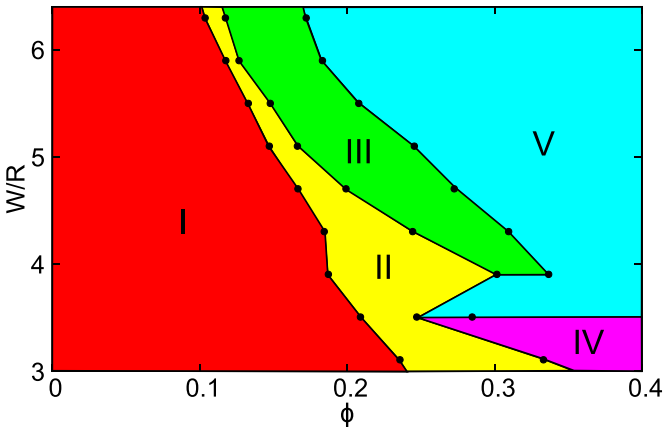

FIG. 10. Phase diagram of different ordering patterns by varying concentration and confinement for viscosity contrast equal to 1.

suspension. The initial random configuration tends to a stable state with an equilibrium interdistance (as discussed before) between two neighbors after some time. At a larger concentration, in the semidilute regime, insertion of a new vesicle between two vesicles that are initially separated by the equilibrium interdistance of an isolated pair destroys the recirculation zones shown in Figs. 9(a) and 9(b), which results in a lower dissipation. When the concentration further increases, there is no room for addition of new vesicles within the single file. The single-file steady-state solution becomes unstable (see pattern II in Fig. 9). We observe an occurrence of defects in the structure in that case. A slight increase of concentration destroys the single-file solution, which undergoes a bifurcation towards a new permanent regime made either of two files (pattern III) or a file of doublets of vesicles (pattern IV), depending on the confinement, as discussed below.

For a sufficiently weak confinement ($W = 4.7R$ and $W = 6.3R$), we have a transition from a single-file solution to two-file solution (see pattern III in Fig. 9) upon increasing concentration ϕ. The one-file structure splits into two lines which are approximately symmetric with respect to the flow centerline. The two files slide with respect to each other in a quite regular way. In the case of strong confinement ($W = 3.1R$), we observe another stable state, called a doublet file (see pattern IV in Fig. 9). In this case, when the one-file becomes crowded (due to an increase in concentration), there is no room for splitting into two files. Instead vesicles form doublets. Now each doublet can be viewed as a single entity, and the doublets form a regular arrangement. In other words, we have a symmetry-breaking bifurcation from an array of vesicles toward an array of doublets. This type of ordering may be referred to as a superstructure with spatial period doubling. In other words, within the elementary periodicity, we have not only a single vesicle but an internal structure (inducing the denomination "superstructure") made of two cells (doublet).

Higher order superstructures (like triplets, etc.) may possibly form at larger ϕ. However, for the set of concentrations explored in this study, these structures were not observed.

For larger ϕ and for a sufficiently weak confinement ($W = 4.7R$ and $W = 6.3R$), the two-file solution becomes unstable and this order is destroyed in favor of a disordered pattern (pattern V in Fig. 9). In our previous study [51] it was reported that we have observed a three-file solution for some time. However, longer simulations show that the three-file solution is unstable.

Let us now consider the case of $\lambda = 10$. A general observation is that for a sufficiently strong confinement the viscosity contrast plays no special role. Indeed, even if λ is sufficiently large to induce tumbling of weakly confined vesicles, sufficiently strong confinement prevents tumbling [47]. In other words, both for small and large values of λ, vesicles exhibit tank treading [see the case of $W = 5R$ in Fig. 1(a)]. In this case, we obtain the same overall behavior for $\lambda = 1$ and $\lambda = 10$ as shown in Fig. 11. However, for a sufficiently weak confinement and a sufficiently small concentration, we observe a single-file configuration, with some tumbling events accompanied by a relative motion between vesicles as shown by the pattern VI in Fig. 11.

Finally, let us say few words regarding the stability and the periodicity of the single-file order. Note first that the regime of one file for $\lambda = 1$ is wider than that for $\lambda = 10$ (as can be deduced from Figs. 10 and 11). A large value of λ tends to suppress the stability of one-file order especially in the case of weak confinement. In fact, while a single vesicle exhibits tank treading for $\lambda = 10$, the interaction has a tendency to induce tumbling, a mechanism by which order is destroyed. We have analyzed the minimal distance between two neighboring vesicles in the one-file regime just before the file becomes unstable. The minimal distance as a function of W for $\lambda = 1$ and $\lambda = 10$ is presented in Fig. 12. This result shows that the confinement has a minor effect on the minimal distance for $\lambda = 1$, whereas a larger viscosity contrast ($\lambda = 10$) significantly influences that distance. Indeed, the inherent tendency for vesicles to undergo tumbling creates a larger range of action for $\lambda = 10$ than for $\lambda = 1$.

D. Rheology of vesicle suspension

Once the spatial organization has been analyzed, we are in a position to establish a link between this organization and rheology. A property that is commonly of interest for unbounded suspensions

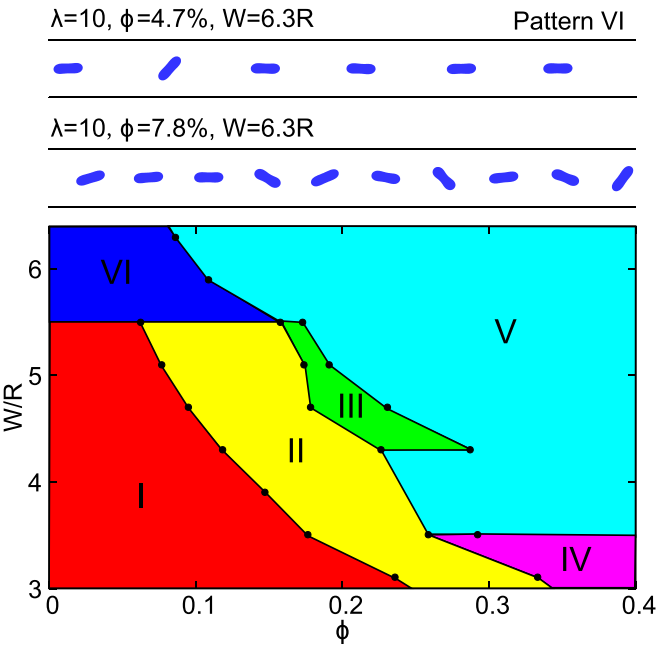

FIG. 11. Top: Configurations of the suspension for pattern VI (tumbling). Bottom: the phase diagram of different ordering patterns by varying concentration and confinement for viscosity contrast $\lambda = 10$.

is the viscosity as a function of the volume fraction ϕ. In the dilute regime, when hydrodynamic interactions between suspended entities can be neglected, the viscosity of suspension takes the generic form $\eta = \eta_{\text{ext}}(1 + \alpha\phi)$, where η_{ext} is the viscosity of the suspending fluid and α is the so-called intrinsic viscosity, which depends on the properties of the suspension. For example, α is equal to 2.5 for rigid spheres (in an unbounded domain), which is the famous Einstein result. α was calculated by Taylor for emulsions [70] and extended to vesicle suspensions more recently [9,71]. When the volume fraction increases, hydrodynamic interactions among suspended entities have to be taken into account, leading to an increase of the suspension viscosity. The classical picture is that there is "jamming" accompanied by a divergence of the viscosity at the maximum volume

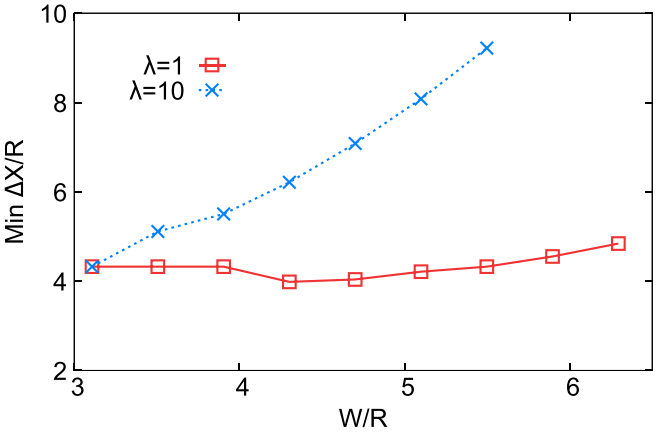

FIG. 12. The minimum interdistance between two neighboring particles.

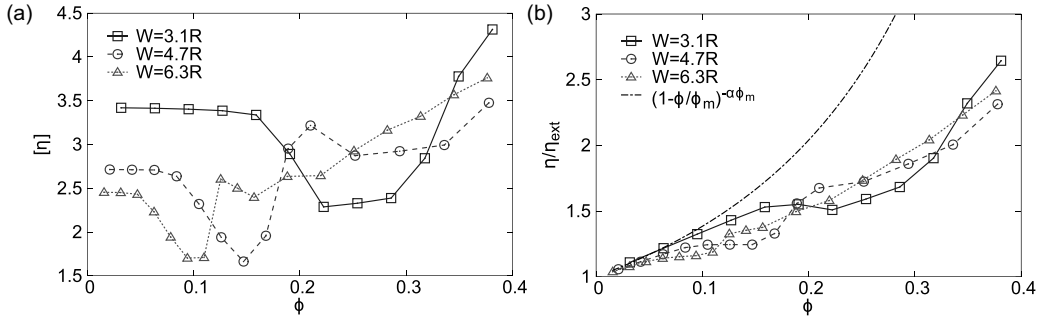

FIG. 13. (a) Normalized viscosity of a suspension of vesicles as a function of concentration for $\lambda = 1$ in different confinements. (b) Effective viscosity of a suspension of vesicles as a function of concentration for $\lambda = 1$ in different confinements. The dot-dashed line shows the viscosity of normal human RBC suspension in unbounded shear flow at low shear rate fitted with the Krieger-Dougherty formula, with $\alpha = 3$ and $\phi_m = 0.67$; see Ref. [73].

fraction ϕ_m corresponding to close packing. A commonly used phenomenological law for rigid particles is that of Krieger and Dougherty $\eta = \eta_{\text{ext}}(1 - \phi/\phi_{\text{ext}})^{-\alpha\phi_m}$ [72]. The normalized viscosity $[\eta] = (\eta - \eta_{\text{ext}})/(\eta_{\text{ext}}\phi)$ increases in a monotonic way with ϕ until it diverges for $\phi = \phi_m$. For a confined vesicle suspension, we show that the order due to the confinement can lead to a very different behavior of the rheology.

1. Dilute and semidilute regimes

First, we investigate the behavior of $[\eta]$ and η with ϕ for $\lambda = 1$ (see Fig. 13). In the dilute regime, the one-file (pattern I) configuration with an equilibrium distance [like Fig. 9(a)] between two neighbors leads to a plateau of $[\eta]$. This means that the effective viscosity η is linear with ϕ for the corresponding concentration as shown by Fig. 13(b). In this regime, the vesicles interact very weakly with each other and this weak interaction is not significantly reflected in the rheology. Note that the dilute regime definition depends on W: The range of concentration for the dilute regime is higher for small W than for large W. As discussed before, the relationship between equilibrium interdistance and confinement is well approximated by $\Delta X^{eq} = 1.47W + 2.42R$ for a pair of vesicles. We have seen that this distance is very close to that between a single vesicle and the center of the closest clockwise vortex created by that vesicle. This means that the vesicle-vesicle interaction is weak. When concentration increases, one expects this distance to evolve (see below), and in this case we can state that vesicle-vesicle interaction starts to play an important role. Thus the quantity $\phi_{tr} = \pi R^2/(W\Delta X^{eq}) = \pi R^2/(1.47W^2 + 2.42RW)$ defines the concentration beyond which vesicle-vesicle interaction becomes relevant. This yields the following concentration range for the dilute regime depending on W: $\phi < 19\%$ for $W = 3.1R$, $\phi < 9\%$ for $W = 4.7R$, and $\phi < 5\%$ for $W = 6.3R$. This is in agreement with the ranges of concentrations where the normalized viscosity shows a plateau regime [Fig. 13(a)].

At a larger concentration, vesicle interaction becomes stronger and we have a crossover from the plateau regime to a regime where $[\eta]$ decreases with ϕ. This is the semidilute regime. An interesting feature is that in the vicinity of the crossover from the plateau regime [Fig. 13(a)] to the descending part of $[\eta]$ can be written as [51] $[\eta] \simeq a_1 + a_2(\phi - \phi_{tr})Y(\phi - \phi_{tr})$, where Y is the Heaviside function and ϕ_{tr} is the crossover concentration. For Fig. 13, $W = 3.1R$, we have $\phi_{tr} \simeq 0.19$, $a_1 \simeq 3.5$, and $a_2 \simeq -22$. This expansion of viscosity is nonstandard as compared to the unbounded regime, in which the expansion is analytical in power of ϕ. This raises naturally the question of whether or not a two-body interaction regime really exists.

We have systematically observed (for $\lambda = 1$) that in the semidilute regime $[\eta]$ decreases in a quasilinear manner [see Fig. 13(a)], while η exhibits a plateau around that concentration [Fig. 13(b)].

This means that the confinement has dramatically altered the rheological behavior. In this regime, increasing ϕ results in a reduction of distance between two neighbors. Each insertion of a new vesicle destroys a large pre-existing vortex and creates a vortex with a smaller amplitude, as shown in Figs. 9(a) and 9(b). This explains the decrease of $[\eta]$ with ϕ. We expect that the smallest normalized viscosity is obtained when the interdistance between two neighbors reaches a minimum, which corresponds to the crossover concentration for which one-file order ceases to be stable. From the refined border of one-file order in Fig. 10, we can get the extent of the semidilute regime, for example, $19\% < \phi < 24\%$ for $W = 3.1R$, $9\% < \phi < 17\%$ for $W = 4.7R$, and $5\% < \phi < 10\%$ for $W = 6.3R$.

2. Concentrated regime

When one-file solution is saturated, an additional vesicle cannot be inserted into the file and wanders in the fluid gap surrounding the file (pattern II in Fig. 9, where we have structural defects). This wandering creates more resistance against the overall flow, and thus $[\eta]$ shows a sudden increase within a very narrow interval of ϕ while η shows a significant increase with ϕ after the plateau regime [Fig. 13(a)]. The saturation of a one-file solution is a precursor for its instability in favor of formation of either doublets (strong confinement, pattern IV in Fig. 9) or of a two-file structure (intermediate confinement, pattern III in Fig. 9). The first case always leads to an increase of $[\eta]$ [$W = 3.1R, \phi > 33\%$ in Fig. 13(a)] because the doublet formation is accompanied by a stronger dissipation within the (thin) fluid gap separating the two vesicles of the doublet [in Fig. 9(d)]. Indeed, within that gap the two membranes tank tread in opposite directions, which generates a quite significant dissipation. The situation in a weaker confinement [$W = 4.7R$ and $W = 6.3R$ in Fig. 13(a)] is significantly different. When one-file structure is saturated, there is also first a sudden increase of $[\eta]$ in a narrow interval of $\phi \in [17\%, 21\%]$ for $W = 4.7R$ and $\phi \in [10\%, 12\%]$ for $W = 6.3R$, due to wandering of a single vesicle closer to a wall. When ϕ lies beyond this interval, instead of doublet formation (as happens for $W = 3.1R$), the one-file structure splits into two files disposed symmetrically with respect to the centerline. Additional vesicles are inserted into either of the two files, destroying larger vortices in favor of smaller ones [see Fig. 9(c)], precisely as in the regime of a single unsaturated file. This destruction of large-amplitude vortices lowers the dissipation and the normalized viscosity of the two-file regime ($\phi \in [21\%, 25\%]$ for $W = 4.7R$ and $\phi \in [12\%, 16\%]$ for $W = 6.3R$) shows a decrease with ϕ. For a weak confinement, the ordered nature of the suspension is less pronounced when ϕ is further increased. The prevailing structure is ultimately disordered.

3. The behavior of the effective viscosity

Hitherto, we have presented the behavior of the normalized viscosity, which shows ample variation with concentration. Let us now analyze the viscosity itself (the effective viscosity η/η_{ext}). The effective viscosity [Fig. 13(b)] shows two interesting features that need to be highlighted. The first feature is that there are regimes (in which order prevails) in which the viscosity remains quasiconstant with ϕ. For example, for the case $W = 3.1R$ in Fig. 13(b), the viscosity remains almost constant when varying the concentration from $\phi \simeq 0.18$ up to $\phi \simeq 0.22$. This is traced back to the fact that the suspension organizes in a subtle way, such that addition of new vesicles leads, in principle, to an increase in the total viscosity, but at the same time the vortices between vesicles are destroyed, leading to lower dissipation. These two effects tend to compensate each other in this concentration interval. The second observation, which is not fully disconnected from the first one, is that the viscosity increases much less rapidly with ϕ as compared to experimental data on blood viscosity in unconfined geometry [shown as a data fit from the Krieger-Dougherty formula in Fig. 13(b)].

4. Effect of viscosity contrast

In the strong confinement regime ($W = 3.1R$), we always have tank treading and both suspensions exhibit similar behaviors regarding their rheology. It is found (in the cases of $W = 3.1R$ and

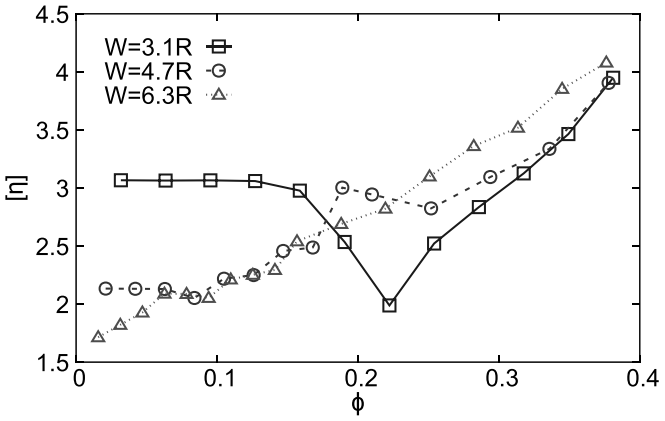

FIG. 14. Normalized viscosity of a suspension of vesicles as a function of concentration for $\lambda = 10$ in different confinements.

$W = 4.7R$) that the normalized viscosity for $\lambda = 10$ is smaller than for $\lambda = 1$ in the one-file configuration regime (small enough ϕ). This result might, at first glance, seem counterintuitive since the fluid inside the vesicles is more viscous. This is due to the fact that the tank-treading angle for $\lambda = 10$ is smaller than that for $\lambda = 1$ so that the vesicles are more aligned with the flow for $\lambda = 10$. This explains the origin of the lower dissipation and thus of a smaller viscosity.

Note also that for $W = 4.7R$, $[\eta]$ does not show a collapse with ϕ after the plateau. As we discussed in Fig. 12, the high viscosity contrast causes instability of one-file order, which leads to a larger interdistance for larger W, reducing the collapse of $[\eta]$. For $W = 6.3R$, because of this instability (due to tumbling, pattern VI), the normalized viscosity exhibits a less pronounced plateau (Fig. 14), in contrast to stronger confinement ($W = 3.1R$ and $W = 4.7R$) where the plateau is more visible. Finally, in the quite concentrated regime, say for $\phi > 30\%$, the prevailing configurations are disordered and $[\eta]$ increases with ϕ regardless of the value of the viscosity contrast.

5. Summary of the link between vesicle organization and rheology

Finally, let us summarize the link between the viscosity behavior as a function of ϕ and the dynamics and the organization of vesicles. For that purpose, we have analyzed the interdistance as a function of concentration. For weak concentration, the interdistance is independent of ϕ. That is, each additional vesicle behaves as a test vesicle in the field of other vesicles. The new added vesicle does not react on the flow field of the other vesicles (and vice versa). The interdistance shows a plateau (Fig. 15), and so does the effective viscosity. For higher concentration, the insertion of a new vesicle destroys the recirculation pattern between two pre-existing vesicles [as shown in Figs. 9(a) and 9(b). When this happens the viscosity $[\eta]$ collapses, expressing a decrease of dissipation associated with the suppression of the recirculation zones. Increasing the concentration further causes the single file to be saturated and a newly added vesicle wanders outside the centerline increasing, thereby resistance to the flow. As a consequence $[\eta]$ increases suddenly. Beyond a certain concentration, the single file splits into two symmetric files, and each file behaves as a single file regarding the reduction of dissipation when a new vesicle is inserted before saturation. $[\eta]$ then decreases, until a critical concentration, at which a new vesicle cannot fit within the two files. In Ref. [51], mention to three-file organization was made, and this structure survived for more than 100 τ_c (τ_c is the vesicle relaxation time scale). Longer simulations showed that this structure is destroyed with time. In LBM, we could occasionally see these types of structures as transients but small perturbations led to disorder. As a consequence, when the two-file structure

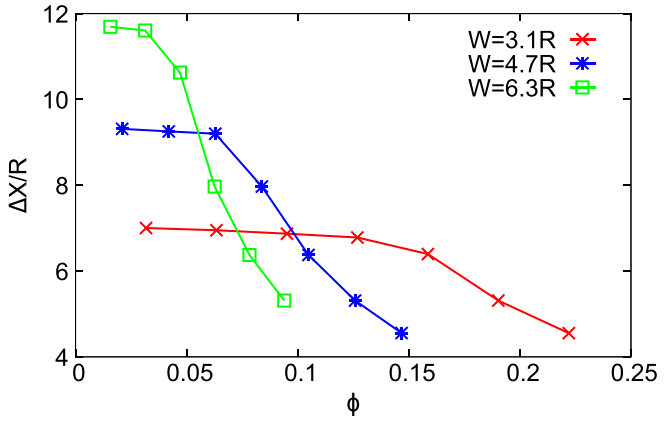

FIG. 15. The distance between two neighboring vesicles as a function of concentration for $\lambda = 1$ for different confinements.

becomes unstable, the normalized viscosity increases monotonically with concentration as a result of disorder.

V. CONCLUSIONS

We have reported on the spatiotemporal patterns of confined vesicle suspensions and have made a link between this organization and the overall rheology. Rheology shows several nonstandard behaviors, like nonmonotonic variation of the normalized viscosity. Our study was limited to a 2D system, and whether order in 3D (apart from a chain structure [51]) will be manifested or not is an open question that requires a systematic study before drawing more general conclusions. While the normalized viscosity shows quite ample signatures due to ordering and destabilization of files, the effect is a bit hidden in the behavior of η itself, although some plateau regimes are clearly observed. Thus it would be more appropriate in experiments to represent $[\eta]$ in order to detect more clearly the oscillation associated with ordering. However, some caution is necessary even for a linear shear flow. Indeed, when the suspension is not homogeneous (as found here), the notion of an overall effective viscosity is ill defined, since it is often assumed (in many rheological experiments using the cone-plate rheometers) that the shear rate is constant in the gap. Clearly, if the suspension has a certain structure, the shear rate in the gap should exhibit strong inhomogeneities. Therefore, we have to resort to an analysis of local rheology, which is a question of primary importance for any complex fluid (be it confined or not) which exhibits an inhomogeneous structure of the suspended entities (like shear bands, organization of files as found here, etc.). Finally, an important task for future investigations is to study in detail the order-disorder transition. The first step is to introduce appropriate physical quantities to analyze the transition. For example, one has to identify an appropriate order parameter to analyze the loss of stability from order to disorder. Furthermore, the transition is probably progressive, passing first toward a superstructure, before disorder takes place. A possible approach is to study the excitation spectra in the ordered phase and to identify the mode which loses stability when disorder appears, as has been recently done for vesicles in a pressure-driven flow [74]. Another interesting issue is how to extend the usual concepts of thermodynamics (thermodynamical potential as a function of an order parameter) to an open nonequilibrium system. We hope to investigate this matter further in the future.

ACKNOWLEDGMENTS

This work was partially supported by CNES (Centre d'Etudes Spatiales), ESA (European Space Agency) and the French-German university programme "Living Fluids" (Grant CFDA-Q1-14).

[1] M. Abkarian, M. Faivre, R. Horton, K. Smistrup, C. A. Best-Popescu, and H. A. Stone, Cellular-scale hydrodynamics, Biomed Mater **3**, 034011 (2008).
[2] X. Li, P. M. Vlahovska, and G. E. Karniadakis, Continuum- and particle-based modeling of shapes and dynamics of red blood cells in health and disease, Soft Matter **9**, 28 (2012).
[3] A. S. Popel and P. C. Johnson, Microcirculation and hemorheology, Annu. Rev. Fluid. Mech. **37**, 43 (2005).
[4] S. Suresh, Mechanical response of human red blood cells in health and disease: Some structure-property-function relationships, J. Mater. Res. **21**, 1871 (2006).
[5] P. M. Vlahovska, T. Podgorski, and C. Misbah, Vesicles and red blood cells: From individual dynamics to rheology, C. R. Phys. **10**, 775 (2009).
[6] A. Farutin, T. Biben, and C. Misbah, Analytical progress in the theory of vesicles under linear flow, Phys. Rev. E **81**, 061904 (2010).
[7] S. R. Keller and R. Skalak, Motion of a tank-treading ellipsoidal particle in a shear flow, J. Fluid Mech. **120**, 27 (1982).
[8] M. Kraus, W. Wintz, U. Seifert, and R. Lipowsky, Fluid Vesicles in Shear Flow, Phys. Rev. Lett. **77**, 3685 (1996).
[9] C. Misbah, Vacillating Breathing and Tumbling of Vesicles Under Shear Flow, Phys. Rev. Lett. **96**, 028104 (2006).
[10] H. Noguchi and G. Gompper, Fluid Vesicles with Viscous Membranes in Shear Flow, Phys. Rev. Lett. **93**, 258102 (2004).
[11] H. Noguchi and G. Gompper, Swinging and Tumbling of Fluid Vesicles in Shear Flow, Phys. Rev. Lett. **98**, 128103 (2007).
[12] J. M. Skotheim and T. W. Secomb, Red Blood Cells and Other Nonspherical Capsules in Shear Flow: Oscillatory Dynamics and the Tank-Treading-to-Tumbling Transition, Phys. Rev. Lett. **98**, 078301 (2007).
[13] M. Abkarian, M. Faivre, and A. Viallat, Swinging of Red Blood Cells Under Shear Flow, Phys. Rev. Lett. **98**, 188302 (2007).
[14] T. M. Fischer, M. Stohr-Lissen, and H. Schmid-Schonbein, The red cell as a fluid droplet: Tank tread-like motion of the human erythrocyte membrane in shear flow, Science **202**, 894 (1978).
[15] V. Kantsler and V. Steinberg, Transition to Tumbling and Two Regimes of Tumbling Motion of a Vesicle in Shear Flow, Phys. Rev. Lett. **96**, 036001 (2006).
[16] M.-A. Mader, V. Vitkova, M. Abkarian, A. Viallat, and T. Podgorski, Dynamics of viscous vesicles in shear flow, Eur. Phys. J. E **19**, 389 (2006).
[17] P. Bagchi and R. M. Kalluri, Dynamics of nonspherical capsules in shear flow, Phys. Rev. E **80**, 016307 (2009).
[18] T. Biben, A. Farutin, and C. Misbah, Three-dimensional vesicles under shear flow: Numerical study of dynamics and phase diagram, Phys. Rev. E **83**, 031921 (2011).
[19] G. Boedec, M. Leonetti, and M. Jaeger, 3D vesicle dynamics simulations with a linearly triangulated surface, J. Comput. Phys. **230**, 1020 (2011).
[20] J. Clausen and C. Aidun, Capsule dynamics and rheology in shear flow: Particle pressure and normal stress, Phys. Fluids **22**, 123302 (2010).
[21] A. Farutin, T. Biben, and C. Misbah, 3D numerical simulations of vesicle and inextensible capsule dynamics, J. Comput. Phys. **275**, 539 (2014).
[22] Y. Kim and M.-C. Lai, Simulating the dynamics of inextensible vesicles by the penalty immersed boundary method, J. Comput. Phys. **229**, 4840 (2010).
[23] Y. Kim and M.-C. Lai, Numerical study of viscosity and inertial effects on tank-treading and tumbling motions of vesicles under shear flow, Phys. Rev. E **86**, 066321 (2012).
[24] C. Pozrikidis, Numerical simulation of the flow-induced deformation of red blood cells, Ann. Biomed. Eng. **31**, 1194 (2003).
[25] S. K. Veerapaneni, A. Rahimian, G. Biros, and D. Zorin, A fast algorithm for simulating vesicle flows in three dimensions, J. Comput. Phys. **230**, 5610 (2011).
[26] H. Zhao, A. H. Isfahani, L. N. Olson, and J. B. Freund, A spectral boundary integral method for flowing blood cells, J. Comput. Phys. **229**, 3726 (2010).

[27] H. Zhao and E. S. G. Shaqfeh, The dynamics of a non-dilute vesicle suspension in a simple shear flow, J. Fluid Mech. **725**, 709 (2013).
[28] D. Barthès-Biesel, Motion and deformation of elastic capsules and vesicles in flow, Annu. Rev. Fluid Mech. **48**, 25 (2016).
[29] D. A. Fedosov, H. Noguchi, and G. Gompper, Multiscale modeling of blood flow: From single cells to blood rheology, Biomech. Model Mechanobiol. **13**, 239 (2014).
[30] U. Seifert, Configurations of fluid membranes and vesicles, Adv. Phys. **46**, 13 (1997).
[31] G. Danker and C. Misbah, Rheology of a Dilute Suspension of Vesicles, Phys. Rev. Lett. **98**, 088104 (2007).
[32] G. Ghigliotti, T. Biben, and C. Misbah, Rheology of a dilute two-dimensional suspension of vesicles, J. Fluid Mech. **653**, 489 (2010).
[33] P. Bagchi and R. M. Kalluri, Rheology of a dilute suspension of liquid-filled elastic capsules, Phys. Rev. E **81**, 056320 (2010).
[34] P. Bagchi and R. M. Kalluri, Dynamic rheology of a dilute suspension of elastic capsules: Effect of capsule tank-treading, swinging, and tumbling, J. Fluid Mech. **669**, 498 (2011).
[35] Y.-C. Fung, *Biomechanics: Circulation* (Springer Science & Business Media, Berlin, 2013).
[36] G. Breyiannis and C. Pozrikidis, Simple shear flow of suspensions of elastic capsules, Theor. Comput. Fluid Dyn. **13**, 327 (2000).
[37] A. Farutin and C. Misbah, Analytical and Numerical Study of Three Main Migration Laws for Vesicles Under Flow, Phys. Rev. Lett. **110**, 108104 (2013).
[38] X. Grandchamp, G. Coupier, A. Srivastav, C. Minetti, and T. Podgorski, Lift and Down-Gradient Shear-Induced Diffusion in Red Blood Cell Suspensions, Phys. Rev. Lett. **110**, 108101 (2013).
[39] M. H.-Y. Tan, D.-V. Le, and K.-H. Chiam, Hydrodynamic diffusion of a suspension of elastic capsules in bounded simple shear flow, Soft Matter **8**, 2243 (2012).
[40] S. K. Doddi and P. Bagchi, Effect of inertia on the hydrodynamic interaction between two liquid capsules in simple shear flow, Int. J. Multiphase Flow **34**, 375 (2008).
[41] P.-Y. Gires, A. Srivastav, C. Misbah, T. Podgorski, and G. Coupier, Pairwise hydrodynamic interactions and diffusion in a vesicle suspension, Phys. Fluids **26**, 013304 (2014).
[42] E. Lac, A. Morel, and D. Barthes-Biesel, Hydrodynamic interaction between two identical capsules in simple shear flow, J. Fluid Mech. **573**, 149 (2007).
[43] D.-V. Le and K.-H. Chiam, Hydrodynamic interaction between two nonspherical capsules in shear flow, Phys. Rev. E **84**, 056322 (2011).
[44] S. Chien, Shear dependence of effective cell volume as a determinant of blood viscosity, Science **168**, 977 (1970).
[45] S. Chien, S. Usami, R. J. Dellenback, M. I. Gregersen, L. B. Nanninga, and M. M. Guest, Blood viscosity: Influence of erythrocyte aggregation, Science **157**, 829 (1967).
[46] B. Kaoui, J. Harting, and C. Misbah, Two-dimensional vesicle dynamics under shear flow: Effect of confinement, Phys. Rev. E **83**, 066319 (2011).
[47] B. Kaoui, T. Krüger, and J. Harting, How does confinement affect the dynamics of viscous vesicles and red blood cells? Soft Matter **8**, 9246 (2012).
[48] B. Kaoui, R. J. Jonk, and J. Harting, Interplay between microdynamics and macrorheology in vesicle suspensions, Soft Matter **10**, 4735 (2014).
[49] A. Lamura and G. Gompper, Dynamics and rheology of vesicle suspensions in wall-bounded shear flow, Europhys. Lett. **102**, 28004 (2013).
[50] M. Thiébaud and C. Misbah, Rheology of a vesicle suspension with finite concentration: A numerical study, Phys. Rev. E **88**, 062707 (2013).
[51] M. Thiébaud, Z. Shen, J. Harting, and C. Misbah, Prediction of Anomalous Blood Viscosity in Confined Shear Flow, Phys. Rev. Lett. **112**, 238304 (2014).
[52] Y. Davit and P. Peyla, Intriguing viscosity effects in confined suspensions: A numerical study, Europhys. Lett. **83**, 64001 (2008).
[53] W. Fornari, L. Brandt, P. Chaudhuri, C. U. Lopez, D. Mitra, and F. Picano, Rheology of Confined Non-Brownian Suspensions, Phys. Rev. Lett. **116**, 018301 (2016).

[54] P. Peyla and C. Verdier, New confinement effects on the viscosity of suspensions, Europhys. Lett. **94**, 44001 (2011).
[55] S. Chen and G. D. Doolen, Lattice Boltzmann method for fluid flows, Annu. Rev. Fluid Mech. **30**, 329 (1998).
[56] M. M. Dupin, I. Halliday, C. M. Care, L. Alboul, and L. L. Munn, Modeling the flow of dense suspensions of deformable particles in three dimensions, Phys. Rev. E **75**, 066707 (2007).
[57] J. Zhang, P. C. Johnson, and A. S. Popel, An immersed boundary lattice Boltzmann approach to simulate deformable liquid capsules and its application to microscopic blood flows, Phys. Biol. **4**, 285 (2007).
[58] B. Kaoui and J. Harting, Two-dimensional lattice Boltzmann simulations of vesicles with viscosity contrast, Rheol. Acta **55**, 465 (2016).
[59] Z. Guo, C. Zheng, and B. Shi, Discrete lattice effects on the forcing term in the lattice Boltzmann method, Phys. Rev. E **65**, 046308 (2002).
[60] K.-I. Tsubota and S. Wada, Effect of the natural state of an elastic cellular membrane on tank-treading and tumbling motions of a single red blood cell, Phys. Rev. E **81**, 011910 (2010).
[61] K.-I. Tsubota, S. Wada, and T. Yamaguchi, Particle method for computer simulation of red blood cell motion in blood flow, Comput. Methods Programs Biomed. **83**, 139 (2006).
[62] I. Cantat, K. Kassner, and C. Misbah, Vesicles in haptotaxis with hydrodynamical dissipation, Eur. Phys. J. E **10**, 175 (2003).
[63] Z.-G. Feng and E. E. Michaelides, The immersed boundary-lattice Boltzmann method for solving fluid-particles interaction problems, J. Comput. Phys. **195**, 602 (2004).
[64] C. S. Peskin, The immersed boundary method, Acta Num. **11**, 479 (2002).
[65] X. Yang, X. Zhang, Z. Li, and G.-W. He, A smoothing technique for discrete δ functions with application to immersed boundary method in moving boundary simulations, J. Comput. Phys. **228**, 7821 (2009).
[66] Y. Liu, L. Zhang, X. Wang, and W. K. Liu, Coupling of Navier-Stokes equations with protein molecular dynamics and its application to hemodynamics, Int. J. Numer. Meth. Fluids **46**, 1237 (2004).
[67] T. Krüger, F. Varnik, and D. Raabe, Shear stress in lattice Boltzmann simulations, Phys. Rev. E **79**, 046704 (2009).
[68] X. He, Q. Zou, L.-S. Luo, and M. Dembo, Analytic solutions of simple flows and analysis of nonslip boundary conditions for the lattice Boltzmann BGK model, J. Stat. Phys. **87**, 115 (1997).
[69] A. Farutin and C. Misbah, Squaring, Parity Breaking, and Tumbling of Vesicles Under Shear Flow, Phys. Rev. Lett. **109**, 248106 (2012).
[70] G. Taylor, The formation of emulsions in definable fields of flow, Proc. R. Soc. London, Ser. A **146**, 501 (1934).
[71] P. M. Vlahovska and R. S. Gracia, Dynamics of a viscous vesicle in linear flows, Phys. Rev. E **75**, 016313 (2007).
[72] I. M. Krieger and T. J. Dougherty, A mechanism for non-Newtonian flow in suspensions of rigid spheres, Trans. Soc. Rheol. **3**, 137 (1959).
[73] R. Pal, Rheology of concentrated suspensions of deformable elastic particles such as human erythrocytes, J. Biomech. **36**, 981 (2003).
[74] S. H. Bryngelson and J. B. Freund, Capsule-train stability, Phys. Rev. Fluids **1**, 033201 (2016).